

A flexible Eu(III)-based metal–organic framework: turn-off luminescent sensor for the detection of Fe(III) and picric acid†

Cite this: *Dalton Trans.*, 2013, **42**, 12403

Xin-Hui Zhou,^{*a} Liang Li,^a Hong-Hui Li,^a Ao Li,^a Tao Yang^a and Wei Huang^{*a,b}

A metal–organic framework (MOF) $\{[Eu_2(MFDA)_2(HCOO)_2(H_2O)_6] \cdot H_2O\}_n$ (**1**) ($H_2MFDA = 9,9$ -dimethylfluorene-2,7-dicarboxylic acid) has been solvothermally synthesized and structurally characterized. **1** possesses the three-dimensional **pcu** type rod-packing structure with one-dimensional rhombic channels. The framework of **1** can reversibly shrink/swell along the *c* axis upon partial/full release of the water molecules. Correspondingly, the rhombic channels become narrow/large and **1** transforms to narrow-pore **1a**/large-pore **1b**. **1**, **1a** and **1b** have almost the same excitation and emission spectra with the strong characteristic red-light-emission of Eu(III). A high photoluminescence quantum yield of 77% and long luminescence lifetime of around 1.1 ms was observed for **1**. The potential of **1b** for Fe³⁺ ions and PA sensing was studied in DMF through the luminescence quenching experiments, which show **1b** is a potential turn-off luminescent sensory material for the selective detection of Fe³⁺ ions and PA with detection limits of around 10⁻⁷ M for both of them. The fluorescence quenching mechanism for Fe³⁺ ions and PA was also investigated.

Received 25th April 2013,
Accepted 13th June 2013

DOI: 10.1039/c3dt51081f

www.rsc.org/dalton

Introduction

Over the past two decades metal–organic frameworks (MOFs) have undergone rapid development because of their exploitable applications as multifunctional materials in gas storage,¹ catalysis,² magnetism,³ adsorption and separation,⁴ etc.⁵ The permanent porosity within some porous MOFs make them competitive candidates for chemosensors. Firstly, the analytes are possibly preconcentrated in the cavities or channels due to the interactions between the analytes and the micropore walls, therefore a lower detection limit and higher sensing sensitivity could be obtained. Secondly, the tunable micropore shape and size, functional sites such as Lewis basic/acidic sites and open metal sites in the micropores, and micropore properties such as hydrophilicity/hydrophobicity, will certainly result in enhancing the selective recognition capability for the different

analytes. The luminescent properties of MOFs are very sensitive to the environment around the chromophores, for example, Eu³⁺ luminescence is a very sensitive probe of its coordination sphere.⁶ Therefore, luminescent frameworks, particularly lanthanide-based luminescent frameworks, are by far the most widely explored type of MOF sensor to date, and have been used as sensors for the detection of cations and anions, small molecules, gases and vapors, pH value, temperature, and ionizing radiation.⁷

Fe³⁺ ions are very important for most organisms and play a crucial role in many biochemical processes at the cellular level, such as the storage and transport of oxygen to tissues and enzymatic reactions of the mitochondrial respiratory chain. The deficiency and overload of Fe³⁺ ions can induce various disorders such as hemochromatosis, anemia, liver damage, diabetes, heart failure and Parkinson's disease.⁸ Therefore, the monitoring of Fe³⁺ ions in a selective and accurate manner is of high importance. Picric acid, 2,4,6-trinitrophenol (PA) is not only a well-known explosive, an even more violent explosive than its well known counterpart 2,4,6-trinitrotoluene (TNT) even at picomolar concentrations, but also a significant environmental pollutant due to its wide use in the leather, pharmaceutical, and dye industries and the manufacture of explosives and rocket fuels. Therefore, the reliable and accurate detection of PA has great significance to homeland security and environmental protection.⁹ However, to the best of our knowledge, there have been few reports of MOFs used

^aKey Laboratory for Organic Electronics and Information Displays (KLOEID) and Institute of Advanced Materials (IAM), Nanjing University of Posts and Telecommunications (NUPT), Nanjing, 210023, P. R. China. E-mail: iamxhzhou@njupt.edu.cn

^bJiangsu-Singapore Joint Research Centre for Organic/Bio-Electronics and Information Display and Institute of Advanced Materials (IAM), Nanjing University of Technology, Nanjing, 211816, P. R. China. E-mail: iamwhuang@njupt.edu.cn

†Electronic supplementary information (ESI) available: The thermogravimetric curves, fluorescence decay curves, excitation and emission spectra. CCDC 918148. For ESI and crystallographic data in CIF or other electronic format see DOI: 10.1039/c3dt51081f

to detect Fe^{3+} ions and only one report for PA sensing very recently.¹⁰

The fluorene molecule and its derivatives are excellent electron donors,¹¹ and have been extensively incorporated into fluorescence conjugated polymers, which demonstrated high sensing performance due to the “molecular wire” effect.¹² Herein, based on the 9,9-dimethylfluorene-2,7-dicarboxylic acid (H_2MFDA) ligands, we synthesized a highly efficient Eu-based luminescent MOF, $\{[\text{Eu}_2(\text{MFDA})_2(\text{HCOO})_2(\text{H}_2\text{O})_6]\cdot\text{H}_2\text{O}\}_n$ with a quantum yield of 77% (the highest $^5\text{D}_0$ quantum yield reported for solid-state Eu(III) compounds with organic ligands in MOFs is 83%),¹³ and investigate the ability of its dehydrated form **1b** for Fe^{3+} ions and PA sensing through luminescence quenching experiments.

Experimental

Materials

All reagents and solvents were used as received from commercial suppliers without further purification. H_2MFDA was synthesized according to the literature.¹⁴

Synthesis of $\{[\text{Eu}_2(\text{MFDA})_2(\text{HCOO})_2(\text{H}_2\text{O})_6]\cdot\text{H}_2\text{O}\}_n$ (**1**)

A mixture of H_2MFDA (0.1 mmol, 28.2 mg), $\text{Eu}(\text{NO}_3)_3\cdot 6\text{H}_2\text{O}$ (0.1 mmol, 44.7 mg), DMF (5 mL), $\text{CH}_3\text{CH}_2\text{OH}$ (2 mL) and H_2O (1 mL) was sealed in a 25 mL Teflon-lined bomb and heated at 120 °C for 3 d. The reaction mixture was slowly cooled to room temperature. Colorless rod-like crystals of **1** suitable for single crystal X-ray diffraction analysis were isolated in 56% yield. Elemental analysis (%) calcd for $\text{C}_{36}\text{H}_{40}\text{Eu}_2\text{O}_{19}$: C, 40.01; H, 3.73%. Found: C, 40.46; H, 3.58%. IR (KBr, cm^{-1}): 550 w, 678 w, 779 s, 1110 w, 1385 vs, 1431 s, 1550 s, 1585 s, 1654 s, 2961 w, 3421 m.

Single-crystal X-ray measurements

X-Ray diffraction data of complex **1** were collected on a Bruker Smart Apex CCD area detector diffractometer using graphite-monochromated Mo-K α radiation ($\lambda = 0.71073$ Å) at room temperature. Cell parameters were retrieved using SMART software and refined using SAINT¹⁵ on all observed reflections. Data were collected using a narrow-frame method with scan widths of 0.30° in ω and an exposure time of 15 s per frame. The highly redundant data sets were reduced using SAINT¹⁵ and corrected for Lorentz and polarization effects. Absorption corrections were applied using SADABS supplied by Bruker.¹⁶ Structure was solved by direct methods using the SHELX-97 program package.¹⁷ The positions of the metal atoms and their first coordination spheres were located from direct-method E maps; other non-hydrogen atoms were found using alternating difference Fourier syntheses and least-squared refinement cycles and, during the final cycles, were refined anisotropically. Hydrogen atoms were placed in calculated positions and refined as riding atoms with a uniform value of U_{iso} . Crystallographic details for **1** have been summarized in Table 1. The CCDC reference number for **1** is 918148.

Table 1 Crystallographic data for complex **1**

Formula	$\text{C}_{36}\text{H}_{40}\text{Eu}_2\text{O}_{19}$	Z	2
Fw	1080.60	D_{calcd} (g cm^{-3})	1.353
Crystal system	Orthorhombic	T/K	293(2)
Space group	$Pnna$	μ (mm^{-1})	2.402
a (Å)	10.4385(14)	$F(000)$	1068
b (Å)	27.184(2)	Reflections collected	8916
c (Å)	9.3482(9)	Unique reflections	2346
α ($^\circ$)	90.00	$R_{\text{int}}, R_{\text{sigma}}$	0.0612, 0.0586
β ($^\circ$)	90.00	GOF (F^2)	1.075
γ ($^\circ$)	90.00	R_1^a, wR_2^b ($I > 2\sigma(I)$)	0.0774, 0.2045
V (Å ³)	2652.6(5)	R_1^a, wR_2^b (all data)	0.1126, 0.2317

$$^a R_1 = \sum \|F_o\| - |F_c| / \sum \|F_o\|. \quad ^b wR_2 = [\sum w(F_o^2 - F_c^2)^2 / \sum w(F_o^2)]^{1/2}.$$

Photoluminescence measurements

The photoluminescence properties of **1**, **1a** and **1b** were investigated in the solid state and/or in N,N -dimethylformamide (DMF) emulsions at room temperature. The **1b**-DMF emulsions were prepared by introducing 3 mg of **1b** powder into 3.00 mL of DMF and then completing ultrasonic agitation for 30 min before testing. Photoluminescent spectra were measured using a RF-5301PC spectrofluorometer.

Other physical measurements

Elemental analyses for C and H were performed on a Perkin-Elmer 240C analyzer. Infrared spectra were recorded on a Vector22 Bruker Spectrophotometer with KBr pellets in the 400–4000 cm^{-1} regions. The powder XRD (PXRD) patterns were recorded on a Shimadzu XD-3A X-ray diffractometer. TGA (thermal gravimetric analysis) was collected on a Shimadzu DTG-60 under 15 mL min^{-1} nitrogen gas flow. Time-resolved fluorescence measurements were performed using a Life-Spec-ps fluorescence lifetime analytical spectrometer (Edinburgh Instruments F900). The absolute quantum yield data were collected on solid samples mounted on quartz slides. The samples were placed within an integrating sphere and excited at 335 nm.

Results and discussion

Crystal structure

The asymmetric unit of **1** contains a Eu(III) ion lying on a twofold axis, a half of a MFDA ligand with C(8) lying on another twofold axis, half of a formate ion, one and a half coordinated water molecules and a quarter of a lattice water molecule (Fig. 1). The formate ligands should be obtained *in situ* during the solvothermal reaction due to the decomposition of DMF. Site occupancy disorder is found in the crystal structure and O(4W) from the water molecule and O(4) from the formate ion occupy the same site with 50% : 50% site occupancies. The Eu(1) ion is eight-coordinated by eight oxygen atoms, four of which are from four MFDA ligands, two from two water molecules and last two from water and/or formate. The Eu–O bond lengths in **1** are comparable to those reported for other Eu–O donor complexes.^{18–20} O(1), O(2), and C(1)–C(8) lie in an approximate plane with the largest deviation of

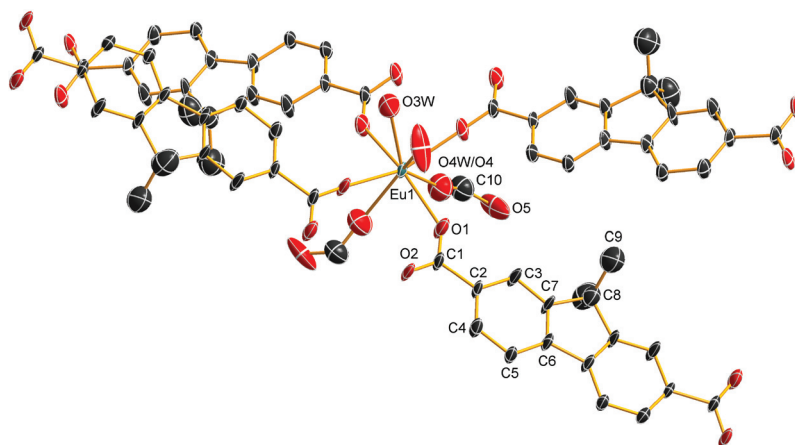


Fig. 1 View of the coordination environments of the Eu(III) ion in **1** with the thermal ellipsoids drawn at the 30% probability level. All H atoms and the noncoordinated water molecule are omitted for clarity.

0.0408 Å for the C(3) atom from the mean plane defined by these atoms. The MFDA ligand acts as a μ_4 -bridge to link four Eu(III) ions with each carboxylate oxygen atom coordinating to a Eu(III) ion, respectively. The Eu(III) ions are arranged in linear arrays along the *a* axis. The neighboring two Eu(III) ions in each linear array are double-bridged by two carboxylate groups from two MFDA ligands with two fluorene-2,7-dicarboxylate moieties being almost coplanar, to produce the 1D Eu–O–C rod-shaped secondary building units (SBUs) (Fig. 2). The Eu–O–C rods are linked along the [011] and [0 $\bar{1}$ 1] directions by the 9,9-dimethylfluorene moieties of the MFDA ligands, forming a three-dimensional **pcu** type rod-packing structure with rhombic channels occupied by formate ions and water molecules (Fig. 2). The solvent accessible space for the dehydrated **1** is 768.57 Å³ per unit cell or 29% of the total volume, calculated using the PLATON routine.²¹

Evaluation of the structural flexibility and thermal stability

1 is prone to lose water molecules when exposed to the air, and its powder X-ray diffraction band corresponding to the (011) and (0 $\bar{1}$ 1) crystal planes at $2\theta = 10.04^\circ$ gradually gets weaker, even disappearing. Simultaneously, a new band at 11.08° is observed, indicating the decrease in the interplanar distance from $d_{011} = d_{0\bar{1}1} = 8.84$ Å to 7.99 Å according to the Bragg equation. The framework is compressed along the *c* axis, the rhombic channels in which become narrow, and this narrow-pore form of **1** is designated as **1a**. This behavior is reversible upon soaking **1a** in water. While when **1** is heated at 100 °C in a vacuum drying oven for 24 hours, the band shifts from 10.04° to 9.46° , indicating the increase in the interplanar distance with $d_{011} = d_{0\bar{1}1} = 9.35$ Å. The framework is stretched along the *c* axis, the rhombic channels in which become large, and this large-pore form of **1** is designated as **1b**. This behavior is also reversible upon soaking **1b** in water. Furthermore, **1a** can also be transformed to **1b** when heated at 100 °C in a vacuum drying oven, however, this behavior is irreversible (Fig. 3). TGA measurements revealed that **1** underwent a weight loss of 12.7% in the temperature range of 20–255 °C,

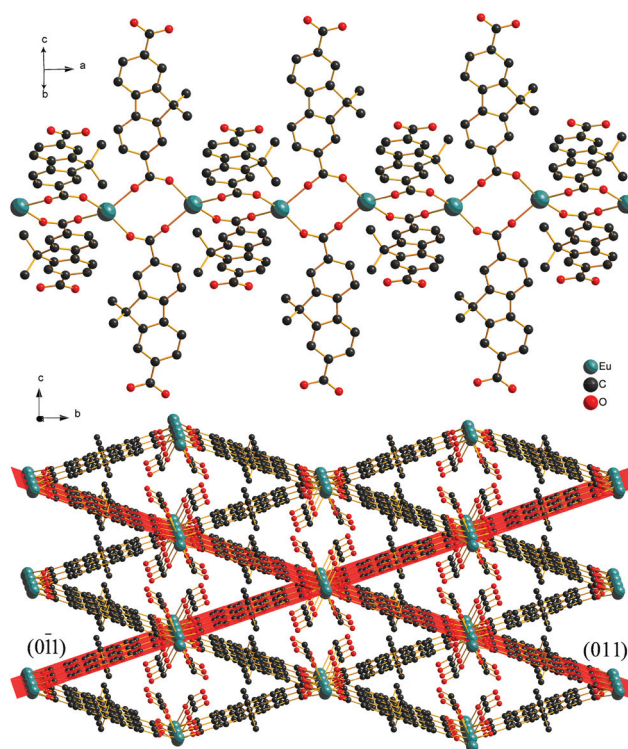


Fig. 2 The three dimensional architecture of **1**. Hydrogen atoms and water molecules are omitted for clarity.

corresponding to the release of seven water molecules (calculated value of 11.7%). While in the same temperature range, the weight losses are 8.2% for **1a** and 0.4% for **1b** (Fig. S1†). It can therefore be speculated that **1a** and **1b** are the partially and fully dehydrated products of **1**, respectively. The stability of **1**, **1a** and **1b** in DMF solution are also confirmed by PXRD.

Photoluminescent properties

When monitored under the characteristic emission (614 nm) of the Eu(III) ion, the excitation spectra of **1**, **1a** and **1b** in the

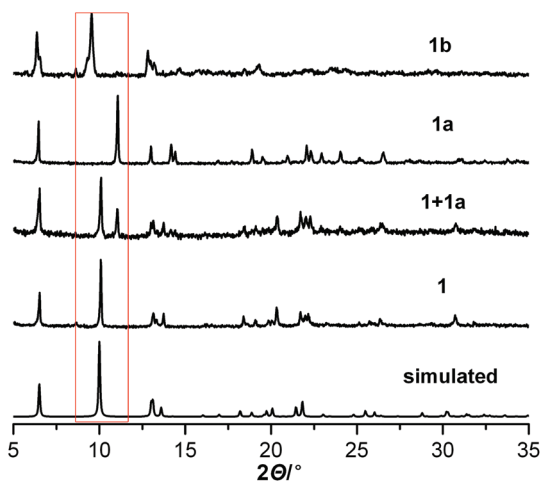


Fig. 3 The powder X-ray diffraction patterns (PXRD).

solid state or dispersed in DMF all exhibit a broad band with a maximum at around 335 nm and two sharp lines at 397 and 466 nm (Fig. S2†). The emission spectra of **1**, **1a** and **1b** excited at 335 nm exhibit the luminescence bands at 580, 592, 614 with shoulder bands at 618, 651 and 700 nm, which could be attributed to the characteristic transitions of the Eu(III) ion: $^5D_0 \rightarrow ^7F_J$ ($J = 0, 1, 2, 3, 4$), respectively (Fig. S2†). The blue light emission in free H_2MFDA ²² completely disappears and the ligands as light-harvesting chromophores (antenna effect) effectively transfer energy to Eu(III) ions with quantum yield of 77.2% for **1**. The decay dynamics of the emission band at 614 nm for **1** and **1b** in air and **1** dispersed in DMF can be well fitted by the monoexponential curve, suggesting one emission center, which is consistent with an independent Eu(III) lattice site in the structure, and their lifetimes are 1.1, 1.1 and 1.2 ms, respectively (Fig. 4). However, **1b** dispersed in DMF displays a biexponential luminescence decay with $\tau_1 = 1.2$ ms (77%) and $\tau_2 = 0.4$ ms (23%), which may be because DMF

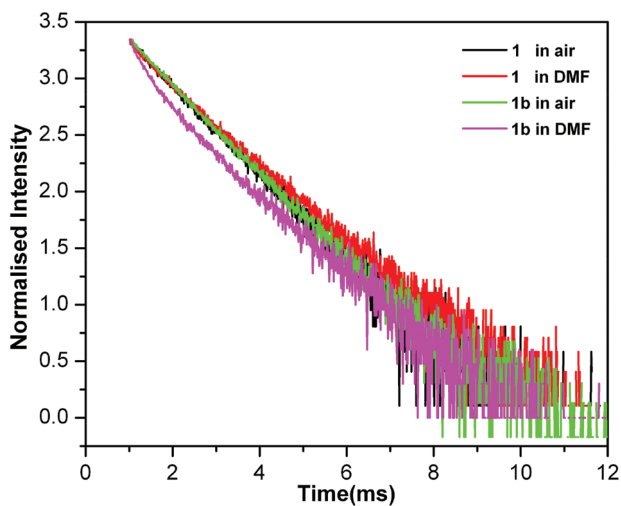


Fig. 4 Semilog plots of fluorescence decay versus time (excited and monitored at 335 nm and 614 nm, respectively).

coordinates to Eu(III) ions located on the surface of crystals resulting in discrepant coordinated environments between the exterior and interior Eu(III) ions. The emission with the shorter luminescence lifetime should be from the exterior Eu(III) ions due to the vibration of the coordinated DMF molecules.

Detection for Fe^{3+} ions

The metal ion interaction studies were performed by addition of nitrate salts of Mg^{2+} , Ca^{2+} , Mn^{2+} , Fe^{3+} , Co^{2+} , Ni^{2+} , Cu^{2+} , Zn^{2+} , Cd^{2+} , Al^{3+} , Cr^{3+} , Gd^{3+} , Er^{3+} and $Hg(CH_3COO)_2$ to **1b**-DMF emulsions, respectively, with the concentration of the metal ion of 1.0×10^{-4} M. Interestingly, the emission spectra exhibited a significant luminescence attenuation with a QP (quenching percentage = $(I_0 - I)/I_0 \times 100\%$, I_0 and I are luminescence intensity of **1b** before and after exposure to the metal ions) of 61% in the presence of Fe^{3+} , while other metal ions displayed insignificant changes with a QP of 20% for Cu^{2+} and lower values of QP for the other 12 metal ions, as displayed in Fig. 5a. This effect reveals that **1b** possesses luminescent turn-off sensing behavior with high selectivity for the Fe^{3+} ion.

To have a better understanding of the luminescence response of **1b** to Fe^{3+} ions, the photoluminescence titration upon the addition of $Fe(NO_3)_3$ to **1b**-DMF emulsions were further conducted and showed that the emission intensity progressively decreased with the increase from 0.01 to 1 mM in the concentrations of the Fe^{3+} ions (Fig. 5b). The detection limit for fluorescence sensing of Fe^{3+} ions was calculated, and the result reveals a value of about 3.3×10^{-7} M.²³ The luminescence titration results can also be treated with the Stern-Volmer equation, $I_0/I = 1 + K_{sv}[Q]$, where K_{sv} is the quenching constant, $[Q]$ is the quencher concentration.²⁴ A nonlinear and upward curve (Fig. 5c) at higher Fe^{3+} ion concentrations suggests that the luminescence quenching mechanism can be attributed to the presence of simultaneous dynamic and static quenching. The dynamic quenching mechanism was governed by the collisional encounters between the fluorene moieties of the MFDA ligand and the electron-deficient Fe^{3+} ions. The static quenching mechanism may be due to the formation of the ground-state non-fluorescent π -electron-metal complexes between Fe^{3+} ions and the fluorene moieties and/or coordination of Fe^{3+} ions with the oxygen atoms from MFDA ligands.^{25,26} The quenching mechanism was further confirmed by the acetylacetone (acac) titration, because the acac can chelate the free Fe^{3+} ions in emulsions and suppress effectively the dynamic quenching. When acac was added to the **1b**-DMF emulsions containing 1.0×10^{-4} M Fe^{3+} ions, with the increase of the concentrations of acac, the emission intensity gradually increased to a maximum value, which was less than that of **1b** before adding the Fe^{3+} ions, and henceforth further added acac to the emulsions, the emission was not further enhanced (Fig. 5d). However, with the increase of the concentration of Fe^{3+} ions up to 1.0×10^{-3} M, the emission of **1b** was completely quenched, and the addition of acac to the emulsions didn't display the luminescence turn-on phenomenon, suggesting that the static quenching plays a more and more

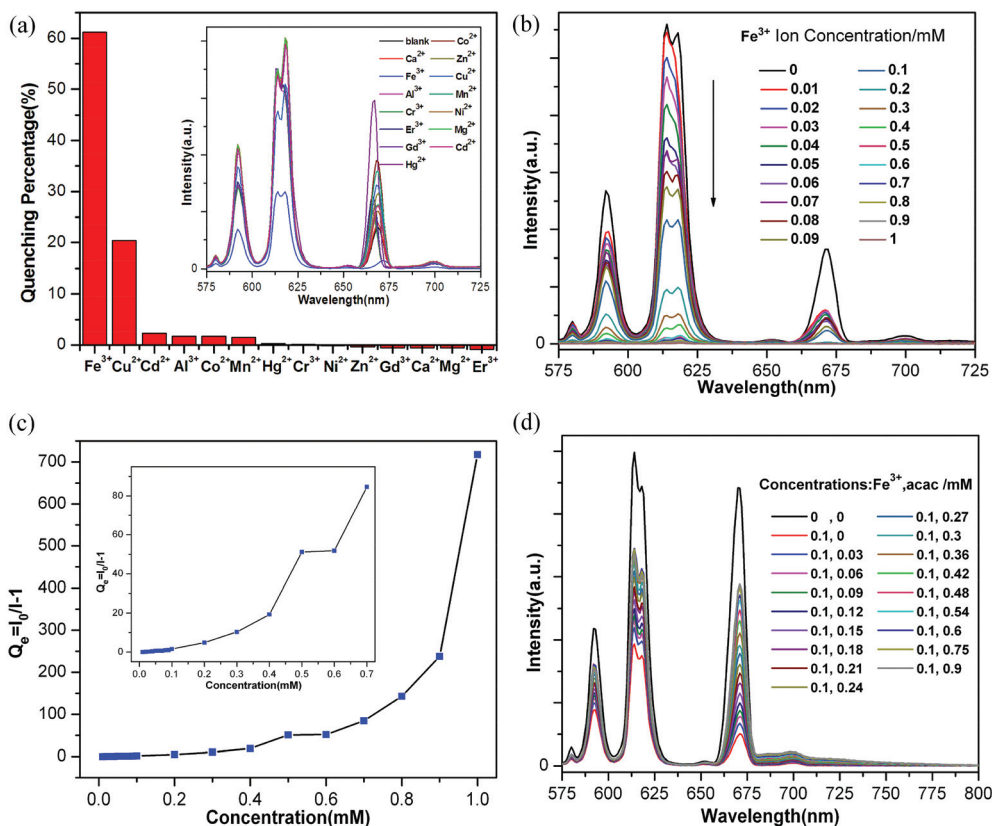


Fig. 5 The luminescence responses of **1b** dispersed in DMF for Fe^{3+} ions: (a) luminescence quenching percentage (insert: emission spectra) in the presence of fourteen different metal ions (each 1.0×10^{-4} M). (b) Concentration-dependent luminescence quenching after adding different concentrations of Fe^{3+} ions. (c) Stern–Volmer plot (insert: the selected area enlarged view) against the concentrations of Fe^{3+} ions. (d) Incomplete luminescence recovery after adding different concentrations of acac into **1b**-DMF emulsions containing 1.0×10^{-4} M Fe^{3+} ions, excited and monitored at 335 nm and 614 nm, respectively. The band around 670 nm is the incident light scattering band.

important role with the increase of the concentration of Fe^{3+} ions.

Detection for nitro compounds

The luminescence responses of **1b** to various nitro compounds were investigated by addition of PA, 2,6-dinitrotoluene (2,6-DNT), 1,3-dinitrobenzene (1,3-DNB), 2-nitrotoluene (2-NT), nitromethane (NM), 2,3-dimethyl-2,3-dinitrobutane (DMNB), 4-nitrotoluene (4-NT), and 2,4-dinitrotoluene (2,4-DNT) to **1b**-DMF emulsions, respectively, with the concentration of the nitro compound being 5.0×10^{-4} M (Fig. 6a). All eight nitro compounds can weaken the photoluminescent intensity of **1b** to a varying degree. The order of quenching efficiency is PA > 2,6-DNT > 2-NT \approx 4-NT \approx 2,4-DNT > 1,3-DNB > DMNB \approx NM. The most effective quencher is PA with QP of 92%, far more than that of 2,6-DNT (29%), and the least effective ones are DMNB and NM with a QP of almost zero, which shows that **1b** is an efficient luminescence sensor for PA with high selectivity.

The sensing performance of **1b** for PA and 2,4-DNT was investigated by the photoluminescence titration experiments, which exhibited that upon addition of PA and 2,4-DNT to **1b**-DMF emulsions, the emission intensity gradually decreased with the increase in the concentrations of the quenchers

(Fig. 6b and 6c). The emission of **1b** was almost completely quenched when the concentration of 2,4-DNT reached 5.0×10^{-2} M, however the value for PA was only 1.0×10^{-3} M, suggesting that PA has greater luminescence quenching efficiency for **1b** than that of 2,4-DNT. The limits of detection for PA and 2,4-DNT are about 4.5×10^{-7} M and 5.4×10^{-6} M,²³ respectively, showing that **1b** as a turn-off luminescent sensory material has greater sensitivity for PA. The luminescence titration results were treated with the Stern–Volmer equation. The linear Stern–Volmer relationship was observed with a K_{sv} of $1.58 \times 10^3 \text{ M}^{-1}$ for 2,4-DNT (Fig. 6c). Therefore, it is speculated that a dynamic quenching process is dominant because the luminescence of **1b** can soon be completely recovered after the removal of 2,4-DNT. For PA, a nonlinear and upward curve (Fig. 6b) at higher concentrations suggested that the fluorescence quenching mechanism can be attributed to the presence of simultaneous dynamic and static quenching. The different fluorescence quenching mechanisms for 2,4-DNT and PA perhaps result from the hydroxyl groups in PA. In order to further elucidate the detection mechanism of the sensors, the luminescence lifetimes of **1b**-DMF emulsions in the absence and presence of PA or 2,4-DNT were measured and remained almost unchanged in different concentrations

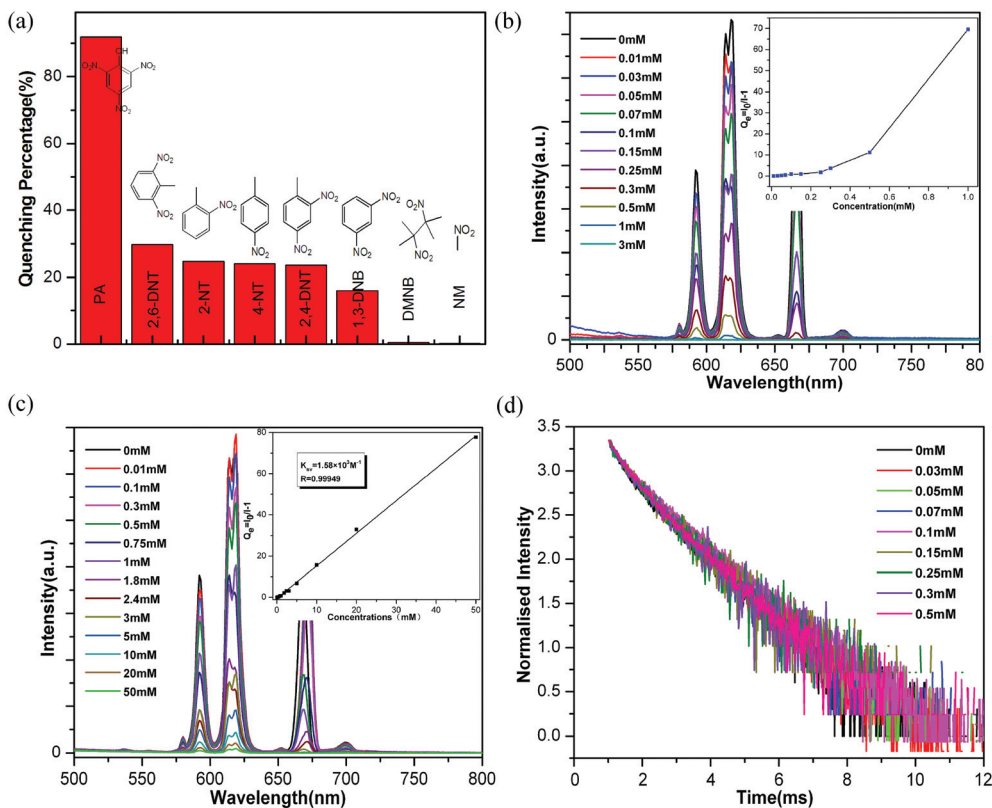


Fig. 6 The luminescence responses of **1b** dispersed in DMF for nitro compounds: (a) luminescence quenching percentage in the presence of eight different nitro compounds (each 5.0×10^{-4} M); Concentration-dependent luminescence quenching after adding different concentrations of (b) PA and (c) 2,4-DNT (insert: Stern–Volmer plot). Semilog plots of fluorescence decay *versus* time in different concentrations of (d) PA, excited and monitored at 335 nm and 614 nm, respectively. The band around 670 nm is the incident light scattering band.

of PA or 2,4-DNT (Fig. 6d and S3[†]), suggesting that there are no interactions between PA or 2,4-DNT and the Eu(III) ions and changes in emission intensity are related to the interactions between PA or 2,4-DNT and the ligands MFDA. Therefore, the quenching behavior for 2,4-DNT was due to the collisional encounters between the fluorene moieties and 2,4-DNT. For PA, the dynamic quenching was due to the collisional encounters between the fluorene moieties and PA, and the static quenching may be due to the hydrogen-bond interactions between the carboxylate groups of MFDA and hydroxyl groups of PA.

Conclusions

In summary, we have obtained a strong red-light-emitting Eu-based MOF $\{[\text{Eu}_2(\text{MFDA})_2(\text{HCOO})_2(\text{H}_2\text{O})_6]\cdot\text{H}_2\text{O}\}_n$ (**1**) (H_2MFDA = 9,9-dimethylfluorene-2,7-dicarboxylic acid) with a high quantum yield of 77% and long luminescence lifetime of around 1.1 ms, which possesses the three-dimensional **pcu** type rod-packing structure with rhombic channels. The framework of **1** is flexible and can reversibly transform to narrow-pore **1a** or large-pore **1b** when **1** is partially or fully dehydrated. The potential of **1b** for Fe^{3+} ions and PA sensing was investigated in DMF and its luminescent emission was turned off in the presence of Fe^{3+} ions or PA with detection limits of around

10^{-7} M for both of them. The sensor showed good selectivity for Fe^{3+} ions with the quenching efficiency being three times larger than those of $\text{Cu}(\text{II})$ and other tested metal ions. The detection limit for PA is an order of magnitude smaller than that for 2,4-DNT, suggesting that the sensor is more suitable for the detection of PA. The fluorescence quenching mechanism for Fe^{3+} ions and PA can be attributed to the presence of simultaneous dynamic and static quenching.

Acknowledgements

This work was supported by the National Natural Science Foundation of China (21001065 and 61106116), the Major State Basic Research Development Program of China (973 Program) (2009CB930600), the Key Project of National High Technology Research of China (2011AA050526), the Natural Science Foundation of the Jiangsu Higher Education Institutions of China (12KJB150017) and Nanjing University of Posts and Telecommunications (NY211068).

Notes and references

- (a) H. C. Zhou, J. R. Long and O. M. Yaghi, *Chem. Rev.*, 2012, **112**, 673; (b) L. J. Murray, M. Dincă and J. R. Long,

- Chem. Soc. Rev.*, 2009, **38**, 1294; (c) R. B. Getman, Y. S. Bae, C. E. Wilmer and R. Q. Snurr, *Chem. Rev.*, 2012, **112**, 703.
- 2 (a) M. Yoon, R. Srirambalaji and K. Kim, *Chem. Rev.*, 2012, **112**, 1196; (b) L. Q. Ma, C. Abney and W. B. Lin, *Chem. Soc. Rev.*, 2009, **38**, 1248; (c) J. Y. Lee, O. K. Farha, J. Roberts, K. A. Scheidt, S. T. Nguyen and J. T. Hupp, *Chem. Soc. Rev.*, 2009, **38**, 1450.
- 3 M. Kurmoo, *Chem. Soc. Rev.*, 2009, **38**, 1353.
- 4 (a) J. R. Li, R. J. Kuppler and H. C. Zhou, *Chem. Soc. Rev.*, 2009, **38**, 1477; (b) D. Zhao, D. J. Timmons, D. Q. Yuan and H. C. Zhou, *Acc. Chem. Res.*, 2011, **44**, 123; (c) K. Sumida, D. L. Rogow, J. A. Mason, T. M. McDonald, E. D. Bloch, Z. R. Herm, T. H. Bae and J. R. Long, *Chem. Rev.*, 2012, **112**, 724.
- 5 (a) D. Farrusseng, *Metal–Organic Frameworks: Applications from Catalysis to Gas Storage*, Wiley-VCH Verlag GmbH & Co. KgaA, 2011; (b) Y. Sakata, S. Furukawa, M. Kondo, K. Hirai, N. Horike, Y. Takashima, H. Uehara, N. Louvain, M. Meilikhov, T. Tsuruoka, S. Isoda, W. Kosaka, O. Sakata and S. Kitagawa, *Science*, 2013, **339**, 193; (c) B. L. Chen, S. C. Xiang and G. D. Qian, *Acc. Chem. Res.*, 2010, **43**, 1115; (d) T. R. Cook, Y. R. Zheng and P. J. Stang, *Chem. Rev.*, 2013, **113**, 734.
- 6 (a) Q. Yue, J. Yang, G. H. Li, G. D. Li and J. S. Chen, *Inorg. Chem.*, 2006, **45**, 4431; (b) C. Serre, F. Millange, C. Thouvenot, N. Gardant, F. Pelléand and G. Férey, *J. Mater. Chem.*, 2004, **14**, 1540.
- 7 (a) J. C. Yuan, F. Y. Yan, D. Q. Guo and L. C. Bang, *Chem. Rev.*, 2012, **112**, 1126; (b) M. D. Allendorf, C. A. Bauer, R. K. Bhaktaa and R. J. T. Houk, *Chem. Soc. Rev.*, 2009, **38**, 1330; (c) L. E. Kreno, K. Leong, O. K. Farha, M. Allendorf, R. P. V. Duyne and J. T. Hupp, *Chem. Rev.*, 2012, **112**, 1105; (d) X. H. Zhou, H. H. Li, H. P. Xiao, L. Li, Q. Zhao, T. Yang, J. L. Zuo and W. Huang, *Dalton Trans.*, 2013, **42**, 5718; (e) J. Rocha, L. D. Carlos, F. A. Almeida Paz and D. Ananias, *Chem. Soc. Rev.*, 2011, **40**, 926.
- 8 L. M. Hyman and K. J. Franz, *Coord. Chem. Rev.*, 2012, **256**, 2333.
- 9 Y. Salinas, R. Martínez-Máñez, M. D. Marcos, F. Sancenón, A. M. Costero, M. Parraad and S. Gil, *Chem. Soc. Rev.*, 2012, **41**, 1261.
- 10 (a) Q. Tang, S. X. Liu, Y. W. Liu, J. Miao, S. J. Li, L. Zhang, Z. Shi and Z. P. Zheng, *Inorg. Chem.*, 2013, **52**, 2799; (b) S. Dang, E. Ma, Z. M. Sun and H. J. Zhang, *J. Mater. Chem.*, 2012, **22**, 16920; (c) M. Zheng, H. Q. Tan, Z. G. Xie, L. G. Zhang, X. B. Jing and Z. C. Sun, *ACS Appl. Mater. Interfaces*, 2013, **5**, 1078; (d) S. S. Nagarkar, B. Joarder, A. K. Chaudhari, S. Mukherjee and S. K. Ghosh, *Angew. Chem., Int. Ed.*, 2013, **52**, 2881.
- 11 K. T. Kamtekar, A. P. Monkman and M. R. Bryce, *Adv. Mater.*, 2010, **22**, 572.
- 12 (a) S. W. Thomas III, J. P. Amara, R. E. Bjork and T. M. Swager, *Chem. Commun.*, 2005, 4572; (b) H. H. Nguyen, X. Z. Li, N. Wang, Z. Y. Wang, J. J. Ma, W. J. Bock and D. G. Ma, *Macromolecules*, 2009, **42**, 921; (c) J. Yang, S. Aschemeyer, H. P. Martínez and W. C. Trogler, *Chem. Commun.*, 2010, **46**, 6804; (d) H. Cavaye, P. E. Shaw, X. Wand, P. L. Burn, S. C. Lo and P. Meredith, *Macromolecules*, 2010, **43**, 10253; (e) T. M. Swager, *Acc. Chem. Res.*, 1998, **31**, 201.
- 13 B. V. Harbuzaru, A. Corma, F. Rey, P. Atienzar, J. L. Jordá, H. Garía, D. Ananias, L. D. Carlos and J. Rocha, *Angew. Chem., Int. Ed.*, 2008, **47**, 1080.
- 14 B. Tsuie, J. L. Reddinger, G. A. Sotzing, J. Soloducho, A. R. Katritzky and J. R. Reynolds, *J. Mater. Chem.*, 1999, **9**, 2189.
- 15 SAINT-Plus, Version 6.02, Bruker Analytical X-ray System, Madison, WI, 1999.
- 16 G. M. Sheldrick, *SADABS An Empirical Absorption Correction Program*, Bruker Analytical X-ray Systems, Madison, WI, 1996.
- 17 G. M. Sheldrick, *SHELXTL-97*, Universität of Göttingen, Göttingen, Germany, 1997.
- 18 X. H. Zhou, Y. H. Peng, Z. G. Gu, J. L. Zuo and X. Z. You, *Inorg. Chim. Acta*, 2009, **362**, 3447.
- 19 X. H. Zhou, Y. H. Peng, X. D. Du, C. F. Wang, J. L. Zuo and X. Z. You, *Cryst. Growth Des.*, 2009, **9**, 1028.
- 20 Y. F. Han, X. Y. Li, L. Q. Li, C. L. Ma, Z. Shen, Y. Song and X. Z. You, *Inorg. Chem.*, 2010, **49**, 10781.
- 21 A. L. Spek, *J. Appl. Crystallogr.*, 2003, **36**, 7.
- 22 S. Q. Su, C. Qin, Z. Y. Guo, H. D. Guo, S. Y. Song, R. P. Deng, F. Cao, S. Wang, G. H. Li and H. J. Zhang, *Cryst-EngComm*, 2011, **13**, 2935.
- 23 G. He, H. N. Peng, T. H. Liu, M. N. Yang, Y. Zhang and Y. Fang, *J. Mater. Chem.*, 2009, **19**, 7347.
- 24 (a) S. W. Thomas III, G. D. Joly and T. M. Swager, *Chem. Rev.*, 2007, **107**, 1339; (b) N. J. Turro, *Modern Molecular Photochemistry*, University Science Books, Sausalito, California, 1991.
- 25 (a) J. R. Lakowicz, *Principles of Fluorescence Spectroscopy*, Springer, New York, 3rd edn, 2006; (b) J. Michon, S. Frelon, C. Garnier and F. Coppin, *J. Fluoresc.*, 2010, **20**, 581; (c) G. Zhang, B. Y. Lu, Y. P. Wen, L. M. Lu and J. K. Xu, *Sens. Actuators, B*, 2012, **171–172**, 786.
- 26 (a) Y. Z. Liao, V. Strong, Y. Wang, X. G. Li, X. Wang and R. B. Kaner, *Adv. Funct. Mater.*, 2012, **22**, 726; (b) L. P. Heng, X. Y. Wang, Y. Q. Dong, J. Zhai, B. Z. Tang, T. X. Wei and L. Jiang, *Chem.-Asian J.*, 2008, **3**, 1041; (c) J. Q. Wang, L. Huang, M. Xue, Y. Wang, L. Gao, J. H. Zhu and Z. G. Zou, *J. Phys. Chem. C*, 2008, **112**, 5014; (d) D. P. Kennedy, C. M. Kormos and S. C. Burdette, *J. Am. Chem. Soc.*, 2009, **131**, 8578.